Load Transient Mitigation for Stand-Alone Fuel Cell Power Generation Systems

Caisheng Wang, *Member, IEEE*, and M. Hashem Nehrir, *Senior Member, IEEE*

***Abstract*—In this paper, a load transient mitigation technique for stand-alone fuel cell (FC)–battery power generation systems is proposed. The technique can be used not only to improve the output power quality of the overall system, but also to mitigate or eliminate the electrical feedback stresses that are caused by load transients upon fuel cells. As a result, the durability of the fuel cell can also be improved. System analysis and controller design procedure for the proposed technique are given in this paper. Simulation studies have been carried out on FC-battery power generation systems using the dynamic models developed for proton exchange membrane fuel cell (PEMFC) and solid-oxide fuel cell (SOFC). Simulation results show the effectiveness of the proposed technique in preventing load transients from affecting the fuel cell performance.**

***Index Terms*—Battery, fuel cell (FC), stand-alone, transient mitigation.**

I. Introduction

THE increasing public awareness of environmental protection and sustainable development has led to increased interest in fuel cell (FC)-based energy sources. Fuel cells are static energy conversion devices that convert the chemical energy of the fuel directly into electrical energy. Compared with conventional power generation systems, they have many advantages, such as high efficiency, zero or low emission (of pollutant gases), and flexible modular structure. FC-based power generation systems are expected to play an important role in future distributed generation (DG) applications. Fuel cell DGs (FCDGs) can either be connected to a utility grid for network reinforcement, or installed in a remote area to supply power as a stand-alone system.

Among different types of fuel cells, the proton exchange membrane fuel cells (PEMFCs) and the solid-oxide fuel cells (SOFCs) show great potential in DG and vehicular applications. They are good energy sources to provide reliable power at a steady rate, but they cannot respond to the electrical load transients as fast as desired. This is mainly due to their slow internal electrochemical and thermodynamic responses [1]. Load transients cause low-reactant condition inside the fuel cells, which is considered to be harmful, and which shortens their life [2]. In order to overcome this problem, fuel cells can be combined with other energy sources with fast dynamics, such as battery or supercapacitor, to form a hybrid power generation system [3]–[6]. The dynamic behavior of a PEMFC and lead-acid battery system was investigated in [3], while no control was discussed in that paper. Fuel cells and supercapacitor banks together with boost dc/dc converters are proposed to achieve a constant output dc voltage [4]. A FC–battery hybrid system is given in [6]; however, the paper concentrates on the design of a new dc/dc converter for fuel cell and battery applications only.

In this paper, a load transient mitigation technique is proposed for stand-alone FC–battery power generation systems. This technique is used to control the system in such a way that during a load transient, the fuel cell provides the steady-state load, and the battery supplies the transient load. The battery voltage is controlled so that it remains within a desired range. Meanwhile, the fuel cell output current ripple is also limited to remain within a certain low range, which is also important for the healthy operation and longer lifetime of the fuel cell [2], [7], [8].

The dynamic models for PEMFC, SOFC, and the lead-acid batteries are briefly described in this paper. Based on these component models and the proposed control technique, simulation studies have been carried out for both PEMFC and SOFC systems to verify the effectiveness of the proposed technique.

II. Component Models

In this section, dynamic models for PEMFC [1] and SOFC [9], and an electrical circuit model for lead-acid batteries [10] are given. For more details on the component model development and model responses, the reader is referred to [1], [9], and [10].

A. PEMFC Model

PEMFCs, one of the most developed fuel cells, show great promise both in transportation and stationary power generation applications. The PEMFC model used in this study is based on the dynamic model for a PEMFC stack, developed and validated in [1]. This physically-based model uses equivalent electrical circuits to represent the electrochemical and thermodynamic phenomena inside the PEMFC. The model was validated by experimental data measured from an Avista Labs SR-12 500-W PEMFC stack. It is an autonomous model operating under constant channel pressure with no control on the input fuel flow into the fuel cell. The fuel cell adjusts the input fuel flow according to its load current keeping the channel pressure constant. Fig. 1 shows the equivalent electrical circuit model for PEMFC, which is developed in [1].

Manuscript received January 27, 2006. This work was supported in part by the NSF Grant ECS-0135229, and in part by the HiTEC Fuel Cell Project at Montana State University, funded by the United States Department of Energy, as a subcontract from Battelle Memorial Institute and Pacific Northwest National Laboratory (PNNL) under Award DE-AC06-76RL01830. Paper no. TEC-00039-2006.

C. Wang is with the Division of Engineering Technology, Wayne State University, Detroit, MI 48202 USA (e-mail: caisheng.wang@gmail.com).

M. H. Nehrir is with the Electrical and Computer Engineering Department, Montana State University, Bozeman, MT 59717 USA (e-mail: hnehrir@ece.montana.edu).

Digital Object Identifier 10.1109/TEC.2006.881081

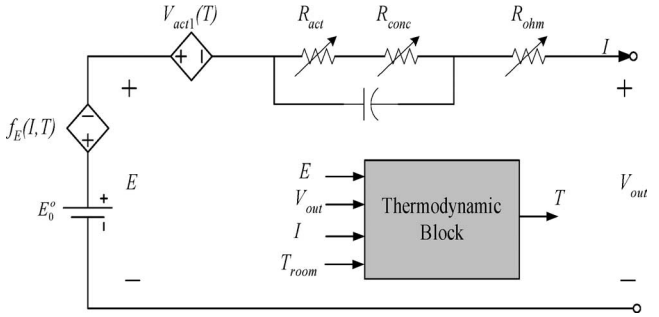

Fig. 1. Electrical circuit model of the PEMFC.

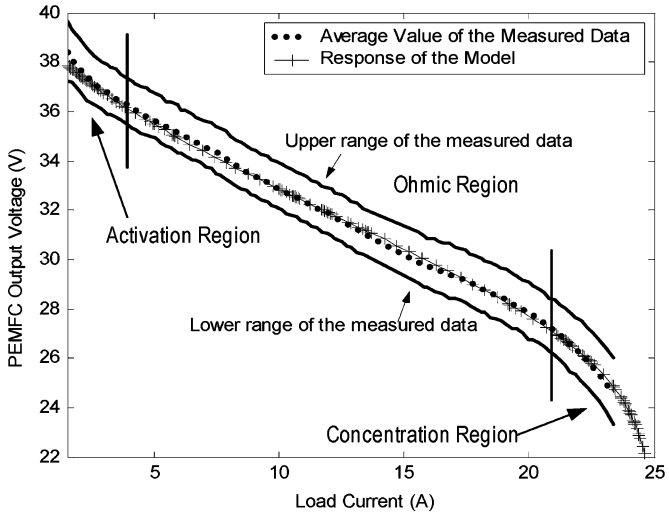

Fig. 2. PEMFC V–I characteristics: comparison of model response with the experimental data [1].

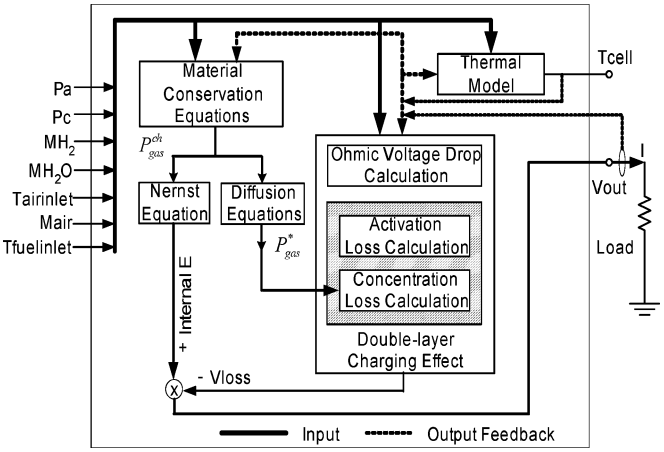

Fig. 3. Block diagram for building the SOFC dynamic model.

In Fig. 1, E is the equivalent internal potential of the fuel cell; E_0° is the standard reference potential of the PEMFC stack at standard temperature and pressure (298 K and 1 atm); $f_E(I,T)$, the current- and temperature-dependent voltage source, is the potential difference due to chemical reactant variations, and fuel and oxidant delay; V_{act1} is the temperature-dependent part of the activation voltage drop; and R_{act}, R_{conc}, and R_{ohm} are the corresponding equivalent resistances of activation, concentration, and ohmic voltage drops inside the fuel cell, respectively. These resistors are current- and/or temperature-dependent [1]. The thermodynamic block in the figure is used to simulate the thermodynamic property inside the fuel cell. T_{room} (room temperature) is one of the four input quantities to the block. The other three input quantities to the thermodynamic block are the fuel cell output current, output voltage, and the internal potential of the fuel cell. The output quantity of this block is the fuel cell temperature (T).

Fig. 2 shows the output voltage versus the load current (V–I) characteristic curve of the 500-W PEMFC model being compared with the experimental data [1]. This characteristic curve can be divided into three regions. The voltage drop across the fuel cell associated with low currents is due to the activation loss inside the fuel cell; the voltage drop in the middle of the curve (which is approximately linear) is due to the ohmic loss in the fuel cell stack; and as a result of the concentration loss, the output voltage at the end of the curve drops sharply as the load current increases.

B. SOFC Mode

In this paper, a physically-based dynamic model for a 5-kW tubular SOFC stack, which is reported in [9], is used for load mitigation study. The model is developed based on the thermodynamic, electrochemical, and material diffusion properties of the fuel cell, and the mass and energy conservation laws. Fig. 3 shows the block diagram of the model. In this model, the input quantities are the anode and cathode pressures (P_{a} and P_{c}), H_2 flow rate (M_{H_2}), H_2O flow rate $(M_{\text{H}_2\text{O}})$, airflow rate (M_{air}), and the initial temperatures of the fuel cell and air ($T_{\text{fuel\_inlet}}$ and $T_{\text{air\_inlet}}$). At any given load current and time, the cell temperature T_{cell} is determined, and both signals are fed back to different blocks contributing to the evaluation of the fuel cell output voltage. The output voltage of SOFC depends on various conditions including fuel composition, fuel flow, oxidant flow, anode and cathode pressures, cell temperature, load current, and the electrical and thermal properties of the cell materials.

The terminal voltage versus current (V–I) curves of the SOFC model at different temperatures are shown in Fig. 4. The activation voltage drop dominates the voltage drop in the low-current region. As the load current increases, the ohmic voltage drop increases fast and dominates in contributing to the voltage drop. When the load current exceeds a certain value (140 A for this SOFC model), the fuel cell output voltage drops sharply due to the concentration voltage drop inside the fuel cell. The dependence of the SOFC performance upon temperature is also illustrated in Fig. 4. The SOFC output voltage is higher at lower temperatures in the low-current zone, while the voltage is higher at higher temperatures in the high-current region. The negative temperature coefficient of the open-circuit internal potential and the temperature-dependent activation voltage and ohmic voltage drops are the main reasons for this kind of temperature-dependent performance of the SOFC model [9].

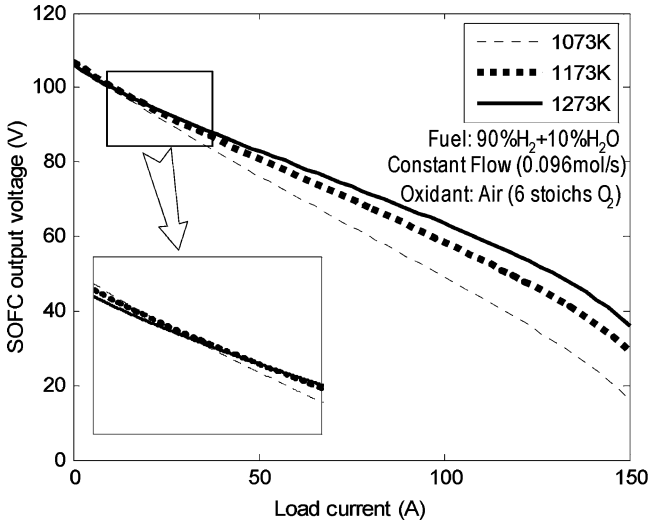

Fig. 4. V–I characteristics of the SOFC mode at different temperatures [9].

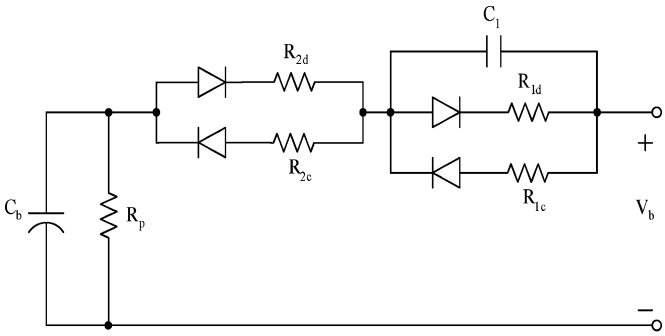

C_b = battery capacitance
R_p = self-discharge resistance, or insulation resistance
R_{2c}= internal resistance for charge
R_{2d}= internal resistance for discharge
R_{1c}= overvoltage resistance for charge
R_{1d}= overvoltage resistance for discharge
C_1 = overvoltage capacitance

Fig. 5. Equivalent circuit model for battery reported in [10].

C. Electrical Circuit Model for the Battery

A validated electrical circuit model for lead-acid batteries, which is shown in Fig. 5, was reported in [10]. All the diodes in the model are ideal, and are used to select different resistances for the charging and discharging states of the battery. The model parameters (capacitances and resistances), which are defined in Fig. 5, are functions of the battery current, and depend on the battery temperature and state-of-charge (SOC) [10], [11]. However, within the voltage range ($100 \pm 5\%$), the difference between the charge and discharge resistances is negligible [10]. For the purpose of analysis, these components are considered constant within the $100 \pm 5\%$ voltage range in this paper. The model shown in Fig. 5 can then be simplified into the circuit model given in Fig. 6. This simplified model is used in this study. The parameters for the 220-V/0.5-kWh battery model are shown in Table I.

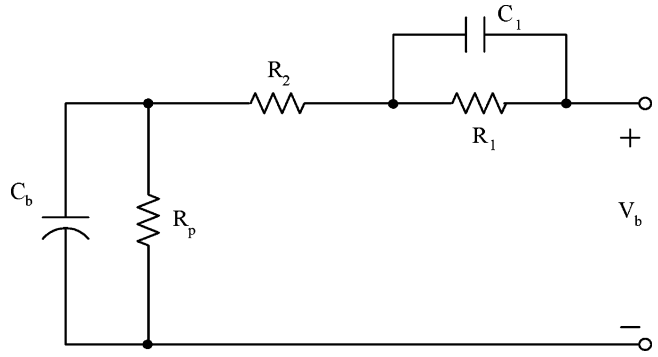

Fig. 6. Simplified circuit model for lead-acid batteries.

TABLE I
PARAMETERS OF THE BATTERY MODEL

C_b	300 F
R_p	25 MΩ
R_2	0.075 Ω
C_1	500 F
R_1	0.1 Ω

III. System Description and Control Strategy

Fig. 7 shows a schematic diagram for the proposed FC–battery power generation system, where a boost dc/dc converter is used to adapt the fuel cell output voltage to the battery voltage (220 V in this paper). Load mitigation has been investigated for both PEMFC- and SOFC-based systems. The models for a 500-W PEMFC and a 5-kW SOFC, which are discussed in Section II, are used to model the FC unit shown in Fig. 7. For the PEMFC-based system studied in this paper, the fuel cell unit consists of four 500-W PEMFC stacks connected in series to provide a 2-kW PEMFC unit. For the SOFC-based system, the fuel cell unit is a single 5-kW SOFC stack. The system load can either be dc or ac (interfaced through an inverter).

A. Load Mitigation Control

Load mitigation control is achieved through a current controller for the dc/dc converter. Given the fact that fuel cells are good energy sources (for providing steady-state power), but not good power sources for transient conditions [1], [3], the purpose of the proposed control strategy is to control the fuel cells so that they supply only steady-state power, while the battery supplies transient power to the load. The load current (I_{load}) is fed back through a low-pass filter to get rid of the high-frequency transients. This filtered load current signal (I_{ref1}) plus the output signal (I_{ref2}) from the battery charging/discharging controller is taken as the reference signal (I_{ref}) to control the dc/dc converter. The output current of the dc/dc converter $(i_{\text{dd\_out}})$ is then compared with the reference signal I_{ref}, and the error signal is processed by the current controller to control the duty ratio of the switch in the converter.

The peak-to-peak ripple of the converter input current (fuel cell output current, $i_{\text{dd\_in}}$ in Fig. 7) should also be controlled to lie within a certain range (10% in this paper) for healthy operation

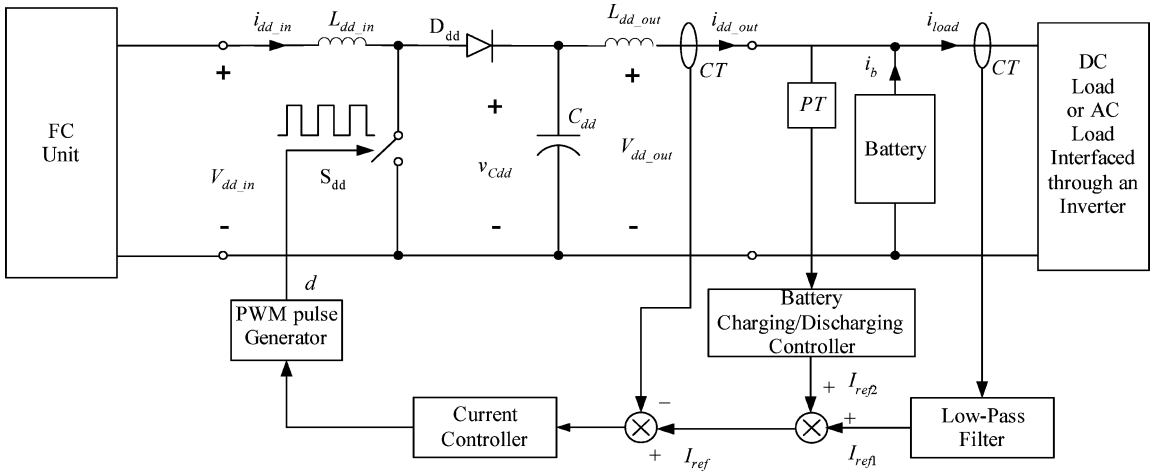

Fig. 7. Schematic diagram of an FC–battery hybrid system with load transient mitigation control.

TABLE II
PARAMETERS OF THE DC/DC CONVERTER

L_{dd_in}	12mH
C_{dd}	2500uF
L_{dd_out}	120mH
f_s (Switch Frequency)	5kHz
k_i	20
k_p	0.02

of the fuel cell [2], [7], [8]. The main components of the dc/dc converter can be selected according to technical specifications, such as the rated and peak voltage and current, the input current ripple, and the output voltage ripple, etc., using the classic design procedure given in [12] and [14]. The component values for the 5-kW dc/dc converter model used in this paper are listed in Table II. The value of the coupling inductor $(L_{\rm dd\_out})$ is selected such that the combination of this inductor with the capacitor $(C_{\rm dd})$ yields a low resonant frequency ($<$10 Hz in this paper) to smoothen out the converter output current $(i_{\rm dd\_out})$.

An approximate state-space model of the converter at the rated operating point can be derived using the averaging technique proposed by Middlebrook and Cúk, which is described in [12]. A PI current controller $(k_{\rm p} + k_{\rm i}/s)$ has been designed for the converter using the classic Bode-plot and root-locus methods [13]. The parameters of the PI current controller are also listed in Table II. The battery charging/discharging controller design and the optimal choice of the filter will be discussed in the following sections.

B. Battery Charging/Discharging Controller

The battery in the system shown in Fig. 7 is designed to buffer transient power. For healthy operation of the battery, its voltage should be within an acceptable range [11]. In order to meet this requirement ($\pm$5% voltage deviation in this paper), a battery charging/discharging controller is designed, as shown in Fig. 8. In this figure, $V_{\rm ref}$ is the rated voltage of the battery (220 V). The regulation constant $K_{\rm c}$ in the figure is determined by assuming that the charging/discharging adjustment of 5% voltage deviation can be achieved in 30 min (1800 s). That is

$$K_{\rm c} = \frac{0.05C_{\rm b}}{1800} \tag{1}$$

where $C_{\rm b}$ is the battery capacitance.

The "normalized" block normalizes the filtered battery voltage deviation $(\Delta V_{\rm dd\_out})$ with respect to the reference voltage $(V_{\rm ref})$. The "|abs|" block gives a nonnegative output $(|\Delta V_{\rm dd\_out}/V_{\rm ref}|)$ regardless of whether $\Delta V_{\rm dd\_out}$ is positive or negative, i.e., whether the battery voltage is higher or lower than the reference voltage. The "relay" block in the figure is a hysteresis block set as follows: It turns "on" (output = 1) when the input is larger than 5%, and remains "on" until the input to the block is less than 0.5%. Otherwise, the output of the relay block is zero. The battery will be charged/discharged at a constant current when its voltage is lower than 95% (higher than 105%) of its rated value. The charging/discharging process will stop when the battery voltage is within 0.5% of its rated value. Therefore, as long as the battery voltage is lower than $0.95V_{\rm ref}$, a positive extra-reference signal

$$I_{\rm ref2} = \frac{0.05C_{\rm b}V_{\rm ref}}{1800} \tag{2}$$

is generated for the current controller. This reference value is maintained until the voltage is higher than $0.995V_{\rm ref}$. However, if the battery voltage is higher than $1.05V_{\rm ref}$, a negative extra-current reference value $[-(0.05C_{\rm b}V_{\rm ref}/1800)]$ is generated, and this value is maintained until the battery voltage is lower than $1.005V_{\rm ref}$. Otherwise, the output of the battery charging/discharging controller is zero.

C. Filter Design

The choice of the low-pass filter needed for the load transient mitigation controller is a tradeoff design between the storage capacity of the battery and the smooth response of the fuel cell to the load transients. Fig. 9 shows an example of the responses of different low-pass filters to a load transient. The damping factors of the filters are all set to 1 in order to avoid any

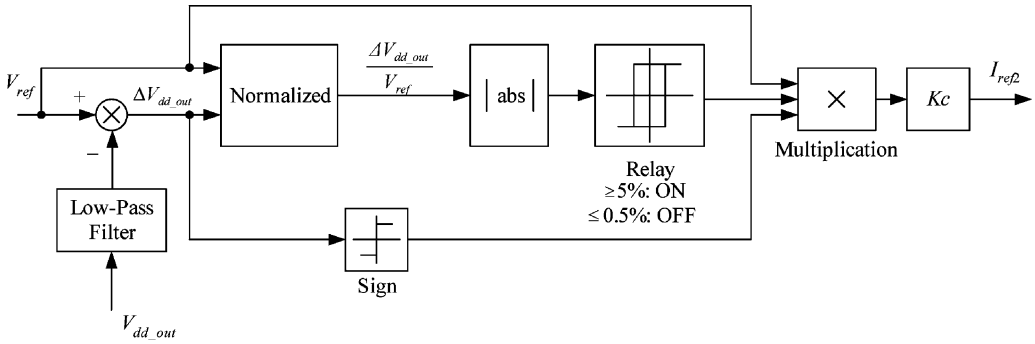

Fig. 8. Schematic diagram of the battery charging/discharging controller.

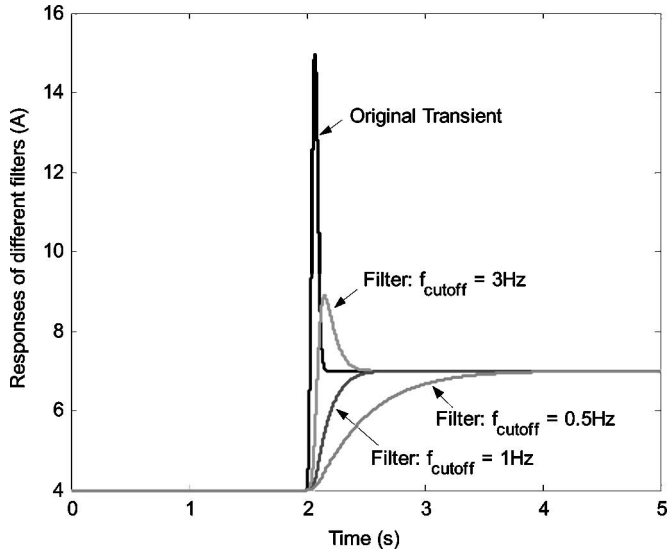

Fig. 9. Example of the responses of different filters to a load transient.

oscillation. It is noted from the figure that the higher the cutoff frequency of the filter, the shorter is the settling time of the response. A filter with shorter settling time requires smaller storage battery capacity, but may cause undesired overshoot. However, the lower the filter cutoff frequency, the longer is the rise time of the filter response, and the smoother the fuel cell response. However, a larger battery capacity is needed if a lower cutoff frequency is chosen for the filter. Therefore, a tradeoff has to be made to choose an optimal filter. In practical applications, one can estimate the fastest possible load transient based on the load information at the location where the fuel cell is to be installed. Transients with frequencies higher than 1250 Hz can be neglected since they do not affect the fuel cell performance significantly [2]. Then, one decides the optimum value (current ripple) that is within the tolerance limit of the fuel cell. An overshoot value of less than 10%, which normally does not cause any significant impact on the fuel cell's healthy operation [2], [7], can be considered to be a good value. The filter can therefore be chosen for the fastest load transient with the highest possible cutoff frequency, while its output overshoot should not exceed a prescribed value (10% suggested in this paper).

IV. Simulation Results

The PEMFC, the SOFC, and the battery models discussed in Section II were used to develop simulation models for a standalone PEMFC–battery and a SOFC–battery power generation system in MATLAB/Simulink using SimPowerSystems blockset. Both systems were controlled by the load transient mitigation technique proposed in Section III. The system performance under load transients was investigated to verify that the power flow is controlled in such a way that the fuel cells only provide steady-state power while the battery supplies transient power to the load. Simulation results on the charging/discharging performance of the battery are also given.

A. Load Transients

For the purpose of verifying the system performance under different load transients, both dc and ac load transients were tested for the PEMFC- and SOFC-based power generation systems. Since the power rating of the PEMFC system studied in this paper is different from that of the SOFC system, different (but similar type of) load transients were used for the two systems.

1) DC Load Transients: The dc load transient due to the starting of a dc motor is used for the simulation study. Fig. 10 shows the load current transient applied to the PEMFC and the SOFC systems when a dc motor is started in three steps. A 2.5-hp/220-V dc motor load is used for the 2-kW PEMFC–battery system, and a 5-kW/220-V dc motor is used for the SOFC system.

2) Ac Load Transients: A general dynamic load model is used to simulate the ac load transients. This model is defined as

$$i(t) = I_0 + I_1 e^{-\alpha_1 t} - I_2 e^{-\alpha_2 t} \tag{3}$$

where I_0, I_1, and I_2 are nonnegative constants, $\alpha_2 > \alpha_1 > 0$, and $i(t)$ is the amplitude of the load current at 60 Hz. In the above equation, it is assumed that the load transient starts at $t = 0$.

These five constant parameters can be determined by

$$\begin{cases} I_0 = i_\infty \\ I_0 + I_1 - I_2 = i_0 \\ \frac{\ln(I_2\alpha_2/I_1\alpha_1)}{\alpha_2 - \alpha_1} = T_{\rm p} \\ I_0 + I_1 e^{-\alpha_1 T_{\rm p}} - I_2 e^{-\alpha_2 T_{\rm p}} = i_{\rm peak} \\ \frac{\ln I_1 - \ln(0.02 I_0)}{\alpha_1} \approx T_{\rm S} \end{cases} \tag{4}$$

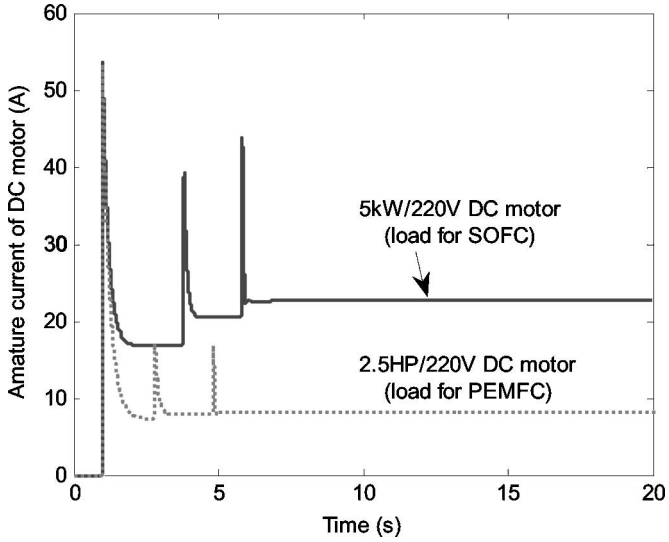

Fig. 10. Load transient of starting a 2.5-hp and a 5-kW/220-V dc motor.

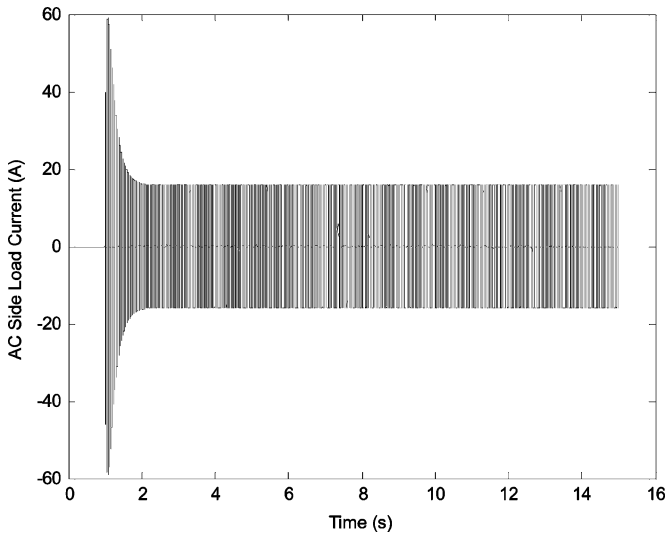

Fig. 11. AC load transient used on the PEMFC–battery system.

where i_0 and i_∞ are the initial and final values of the transient load current, T_p is the time taken by the transient current to reach its peak value (i_peak), and T_S is the settling time (time taken to settle to within $\pm 2\%$ of the final value). Therefore, by specifying i_0, i_∞, i_peak, T_p, and T_S, one can numerically calculate the five parameters in (4). Fig. 11 shows the load transient curve used for the PEMFC system, which starts at 1 s. The parameters of this load transient are $I_0 = 15.84$ A, $I_1 = 79.2$ A $I_2 = 95.04$ A, $\alpha_1 = 5$, and $\alpha_2 = 30$. The parameters of the ac load current transient for the SOFC system under study are $I_0 = 39.6$ A, $I_1 = 198$ A, $I_2 = 237.6$ A, $\alpha_1 = 5$, and $\alpha_2 = 30$, which give the load transient a shape similar to the one shown in Fig. 11, but with a higher magnitude.

B. Load Mitigation

In this section, simulation results are presented for load transient mitigation studies of the PEMFC and SOFC systems. It is assumed throughout that the battery used in the system is fully

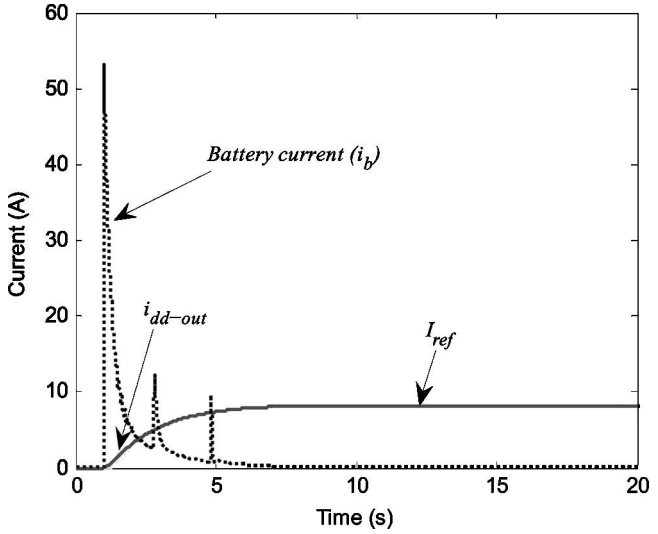

Fig. 12. Reference signal (I_ref) for the current controller, the battery current (i_b), and the converter output current $(i_\mathrm{dd\_out})$ under the load transient for PEMFC shown in Fig. 10.

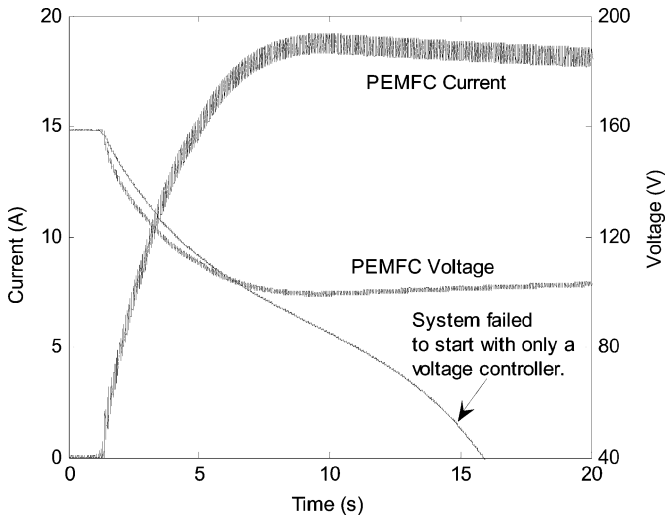

Fig. 13. PEMFC output current and voltage responses to the dc load transient shown in Fig. 10.

charged to its rated voltage, i.e., 220 V, before the application of load transients.

1) PEMFC System: First, the system is tested under the dc motor load transient shown in Fig. 10. The cutoff frequency of the low-pass filter in this simulation is chosen to be 0.1 Hz, and the damping factor is set to 1. The corresponding current reference signal (I_ref in Fig. 7) presented in Fig. 12, shows that the rise time of the filter response to the load transient is less than 10 s, with no overshoot. The battery current (i_b) and the converter output current $(i_\mathrm{dd\_out})$ responding to the load transient current are also shown in Fig. 12. The figure shows that $i_\mathrm{dd\_out}$ follows the reference signal (I_ref) very well, and they almost overlap each other. Further, it is seen that the battery picks up the transient current while the converter output current rises smoothly (as designed) from its previous steady-state to its next steady-state value. The corresponding PEMFC current and voltage responses are shown in Fig. 13. It is noted that the

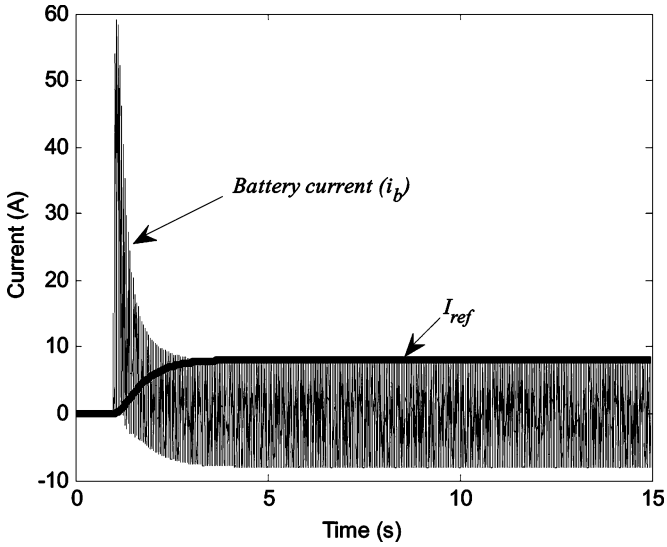

Fig. 14. PEMFC: the control reference signal $(I_{\rm ref})$ and the battery current $(i_{\rm b})$ under the ac load transient shown in Fig. 11.

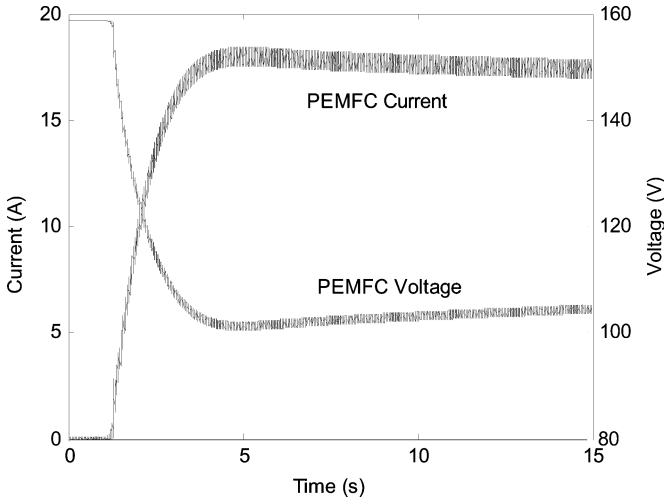

Fig. 15. PEMFC output current and voltage responses to the ac load transient shown in Fig. 11.

PEMFC output varies smoothly during the load transient; the PEMFC is controlled to supply only the steady-state current to the load. It is also noted that the fuel cell current ripple is around 5.5%, which is within the acceptable range (10%).

For the purpose of comparison, a simulation study was carried out on the PEMFC system, shown in Fig. 7, with a typical voltage controller for the dc/dc converter only (i.e., $i_{\rm load}$ and $i_{\rm dd\_out}$ are not fed back in Fig. 7). The controller is used to keep the converter output voltage constant under load variations. Fig. 13 also shows the PEMFC output voltage for this case study when the dc load transient (Fig. 10) is applied to the PEMFC system. It is noted that the system fails to start the dc motor, hence, justifying the need for the current controller.

Figs. 14 and 15 show the simulation results when an ac load transient (Fig. 11) is applied to the PEMFC–battery system. Fig. 14 shows the reference signal $(I_{\rm ref})$ and the battery output current. The corresponding PEMFC output current and voltage

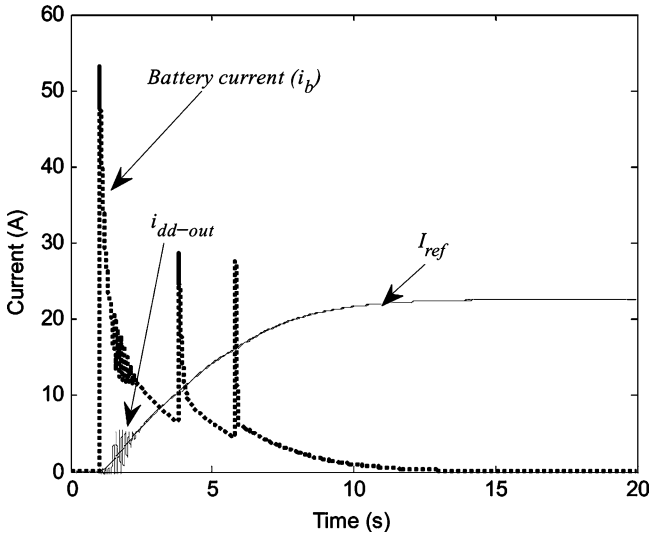

Fig. 16. Reference signal $(I_{\rm ref})$ for the current controller, the battery current $(i_{\rm b})$, and the converter output current $(i_{\rm dd\_out})$ under the load transient for SOFC shown in Fig. 10.

are shown in Fig. 15. The fuel cell output current ripple is around 5.5%, and the voltage ripple is around 2%. It is noted from these figures that the proposed control technique also works well under the ac load transient.

2) SOFC System: Similar to the PEMFC system, the simulation study on the SOFC system under a dc load transient (Fig. 10) is investigated. The cutoff frequency of the low-pass filter is also chosen to be 0.1 Hz, and the damping factor is set to 1. Fig. 16 shows the current reference signal $(I_{\rm ref})$, the battery current $(i_{\rm b})$, and the converter output current $(i_{\rm dd\_out})$ responding to the load transient current. The figure shows that $i_{\rm dd\_out}$ follows the reference signal $(I_{\rm ref})$ very well for the SOFC system. The corresponding SOFC output current and voltage responses are given in Fig. 17, which shows that the SOFC output voltage and current vary smoothly during the load transient. The SOFC is controlled to supply only the steady-state current to the load, and its output current ripple is less than 1.5%, which is much lower than the preset value (10%).

Figs. 18 and 19 show the simulation results when an ac load transient (shown in Fig. 11 but with a different amplitude) is applied to the SOFC system. The reference signal $(I_{\rm ref})$ and the battery output current $(i_{\rm b})$ are given in Fig. 18. It is clear from this figure that the battery responds to the transient part of the load, and the reference signal (for the dc/dc converter) rises smoothly to its new steady-state value. The corresponding SOFC output current and voltage under the ac load transient are shown in Fig. 19. The SOFC output ripple is also very small in this case. Figs. 18 and 19 show that the proposed control technique also works well for the SOFC system under the ac load transient.

C. Battery Charging/Discharging

When the battery voltage lies outside a certain range (±5% in this paper), the battery charging/discharging controller (Figs. 7

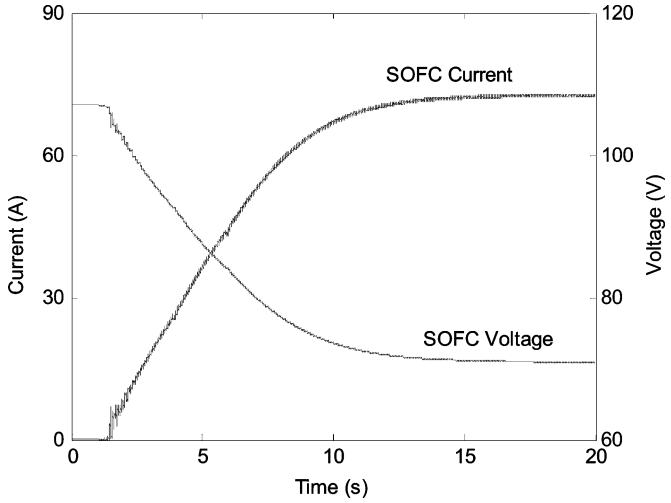

Fig. 17. SOFC output current and voltage responses to the dc load transient shown in Fig. 10.

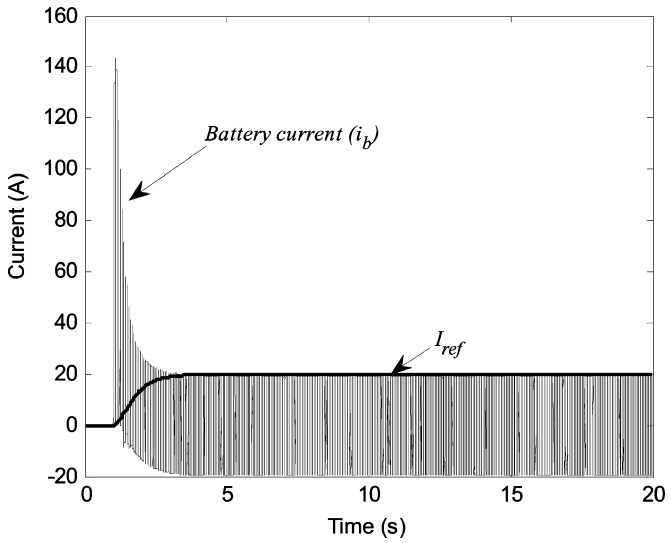

Fig. 18. SOFC: the control reference signal $(I_{\rm ref})$ and the battery current $(i_{\rm b})$ under the ac load transient.

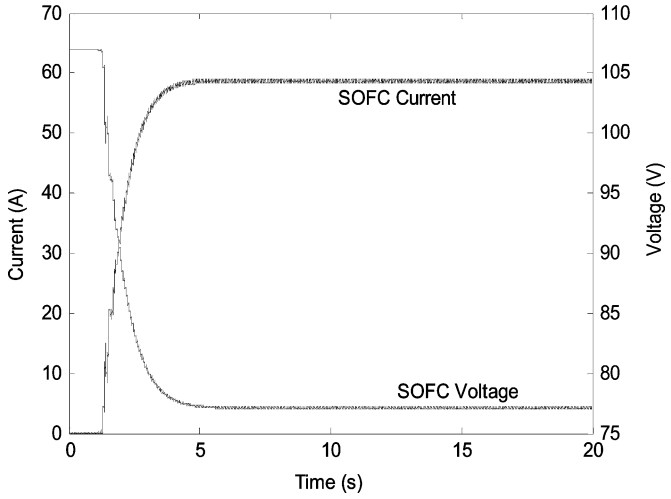

Fig. 19. SOFC output current and voltage responses to the ac load transient.

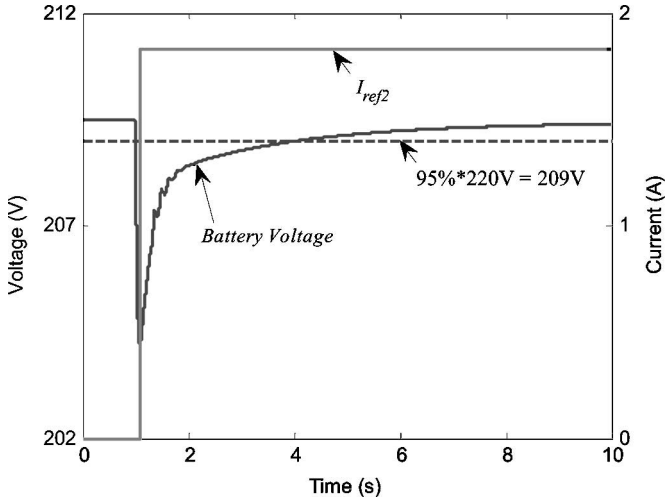

Fig. 20. Battery voltage and extra-current reference $(I_{\rm ref2})$ curves when the battery is being charged.

and 8) starts to operate bringing the battery voltage back within the acceptable range. In practice, the battery normally needs to be charged after a load transient is applied to the FC–battery system. This is because the transient power delivered by the battery to the load, together with the battery self-discharging characteristic, normally causes the battery voltage to drop. If the battery voltage drops below the preset value (95% of the rated voltage of the battery), the battery charging/discharging controller starts to operate charging the battery. Similarly, the battery charging/discharging controller goes into the discharging mode if the battery voltage exceeds its preset limit (105% of the rated voltage of the battery). In this section, simulation results are given for battery charging after the dc motor load transient (described in Section IV) is applied to the SOFC–battery system.

Fig. 20 shows the battery voltage and the extra-current reference ($I_{\rm ref2}$ in Fig. 7) after the load transient is applied to the SOFC–battery system. Before the load transient is applied, the battery voltage is already close to its lower limit (209 V). During the transient, the battery voltage drops below the limit, which triggers the battery charging/discharging controller to start operating and generating a new $I_{\rm ref2}$. This extra-current reference is added to the current reference $(I_{\rm ref1})$ from the current filter to produce the new current reference signal $(I_{\rm ref})$ for the current controller (Fig. 7). Fig. 21 shows the load transient current, the overall current reference signal $(I_{\rm ref})$, the filter output reference signal $(I_{\rm ref1})$, the battery current $(i_{\rm b})$, and the corresponding converter output current $(i_{\rm dd\_out})$. It is clear from Figs. 20 and 21 that during and after the transient load demand, the battery picks up the transient load (battery discharging), and the reference currents ($I_{\rm ref1}$ and $I_{\rm ref}$) slowly increase to bring the fuel cell current to its new steady-state value and also charge the battery (battery charging). This smooth transition

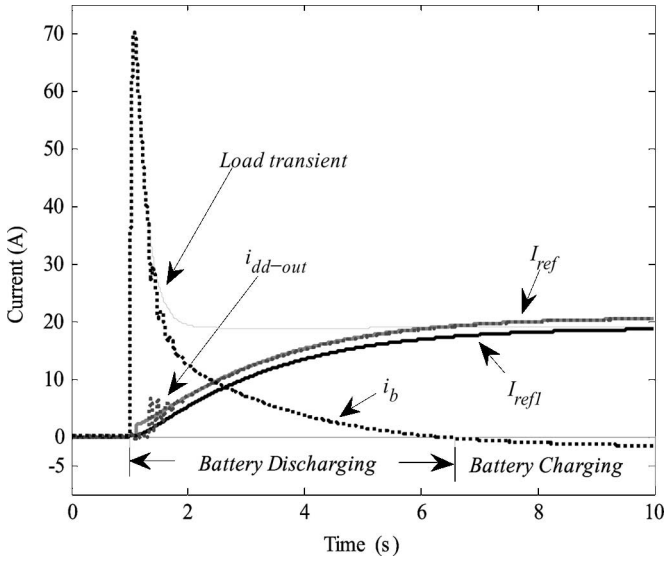

Fig. 21. Load transient, the overall current control reference signal (I_{ref}), the low-pass filter output signal (I_{ref1}), and the corresponding converter output current ($i_{\text{dd\_out}}$) when the battery is being charged.

of the FC current is essential for the improved reliability and durability of fuel cells.

V. Conclusion

In this paper, a load transient mitigation control strategy is proposed for the FC–battery power generation systems. The control strategy consists of a current controller for the dc/dc converter and a battery charging/discharging controller to keep the battery voltage within the desired range. During load transients, the fuel cells are controlled (by the proposed transient mitigation technique) to supply the steady-state power to the load while the battery supplies the transient power to the load. Simulation studies under different load transients are carried out for both the PEMFC and the SOFC systems. Simulation results show that the fuel cell current can be controlled as desired, and the battery voltage can be held within the prescribed range. The results show that the proposed load transient mitigation technique works well for both types of fuel cell systems (PEMFC and SOFC) studied.

Acknowledgment

The authors would like to thank Dr. D. A. Pierre of Montana State University for his comments and suggestions.

References

[1] C. Wang, M. H. Nehrir, and S. R. Shaw, "Dynamic models and model validation for PEM fuel cells using electrical circuits," *IEEE Trans. Energy Convers.*, vol. 20, no. 2, pp. 442–451, Jun. 2005.

[2] R. S. Gemmen, "Analysis for the effect of inverter ripple current on fuel cell operating condition," *Trans. ASME, J. Fluids Eng.*, vol. 125, no. 3, pp. 576–585, May 2003.

[3] J. C. Amphlett, E. H. de Oliveira, R. F. Mann, P. R. Roberge, and A. Rodrigues, "Dynamic interaction of a proton exchange membrane fuel cell and a lead-acid battery," *J. Power Sources*, vol. 65, pp. 173–178, 1997.

[4] D. Candusso, L. Valero, and A. Walter, "Modelling, control and simulation of a fuel cell based power supply system with energy management," in *Proc. IEEE 2002 28th Annu. Conf. Ind. Electron. Soc.*, vol. 2, no. 5–8, pp. 1294–1299.

[5] J. Larminie and A. Dicks, *Fuel Cell Systems Explained*. New York: Wiley, 2001, pp. 362–367.

[6] F. Z. Peng, H. Li, G. Su, and J. S. Lawler, "A new ZVS bidirectional dc–dc converter for fuel cell and battery application," *IEEE Trans. Power Electron*, vol. 19, no. 1, pp. 54–65, Jan. 2004.

[7] K. Acharya, S. K. Mazumder, R. K. Burra, R. Williams, and C. Haynes, "System-interaction analyses of solid-oxide fuel cell (SOFC) power-conditioning system," in *Conf. Rec. 2003 IEEE Ind. Appl. Conf.*, vol. 3, no. 12–16, pp. 2026–2032.

[8] S. K. Mazumder, K. Acharya, C. L. Haynes, R. Williams, Jr., M. R. von Spakovsky, D. J. Nelson, D. F. Rancruel, J. Hartvigsen, and R. S. Gemmen, "Solid-oxide-fuel-cell performance and durability: Resolution of the effects of power-conditioning systems and application loads," *IEEE Trans. Power Electron.*, vol. 19, no. 5, pp. 1263–1278, Sep. 2004.

[9] C. Wang and M. H. Nehrir, "A physically-based dynamic model for solid oxide fuel cells," *IEEE Trans. Energy Convers.*, vol. 22, no. 4, pp. 887–897, 2007.

[10] Z. M. Salameh, M. A. Casacca, and W. A. Lynch, "A mathematical model for lead-acid batteries," *IEEE Trans. Energy Convers.*, vol. 7, no. 1, pp. 93–98, Mar. 1992.

[11] D. Linden, Ed., *Handbook of Batteries*, 2nd ed. New York: McGraw-Hill, 1995.

[12] N. Mohan, T. M. Undeland, and W. P. Robbins, *Power Electronics—Converters, Applications, and Design*. New York: Wiley, 2003.

[13] J. Van de Vegte, *Feedback Control Systems*, 3rd ed. Englewood Cliffs, NJ: Prentice-Hall, 1994.

[14] D. W. Hart, *Introduction to Power Electronics*. Englewood Cliffs, NJ: Prentice-Hall, 1997.

Caisheng Wang (M'02) received the B.S. and M.S. degrees from Chongqing University, Chongqing, China, in 1994 and 1997, respectively, and the Ph.D. degree from Montana State University, Bozeman, in 2006, all in electrical engineering.

From August 1997 to May 2002, he was an Electrical Engineer in Zhejiang Electric Power Test and Research Institute, Hangzhou, China. Since August 2006, he has been a Faculty Member in the Division of Engineering Technology, Wayne State University, Detroit. His current research interests include modeling and control of power systems and electrical machinery, alternative/hybrid energy power generation systems, and fault diagnosis and online monitoring of electric apparatus.

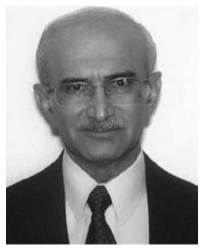

M. Hashem Nehrir (S'76–M'88–SM'89) received the B.S., M.S., and Ph.D. degrees in electrical engineering from Oregon State University, Corvallis, in 1969, 1971, and 1978, respectively.

Since 1987, he has been with the Department of Electrical and Computer Engineering, Montana State University, Bozeman, where he is currently a Full Professor. His current research interests include modeling and control of power systems and electrical machinery, alternative energy power generation systems, distributed generation, and application of intelligent controls to power systems. He is the author of two textbooks and an author or coauthor of numerous technical papers.